The Radial Variation of H I Velocity Dispersions in Dwarfs and Spirals

Ianjamasimanana, R.; de Blok, W. J. G.; Walter, Fabian; Heald, George H.; Caldú-Primo, Anahi; Jarrett, Thomas H.

Published in:
The Astronomical Journal

DOI:
10.1088/0004-6256/150/2/47

Publication date:
2015

The Astronomical Journal, 150:47 (12pp), 2015 August doi:10.1088/0004-6256/150/2/47

THE RADIAL VARIATION OF H I VELOCITY DISPERSIONS IN DWARFS AND SPIRALS

R. Ianjamasimanana[1], W. J. G. de Blok[2,3,4], Fabian Walter[5], George H. Heald[3,4], Anahi Caldú-Primo[5], and Thomas H. Jarrett[2]
[1] College of Graduate Studies, University of South Africa, P.O. Box 392, UNISA 003, South Africa; tianjar@unisa.ac.za
[2] Astrophysics, Cosmology and Gravity Centre, Department of Astronomy, University of Cape Town, Private Bag X3, Rondebosch 7701, South Africa
[3] ASTRON, the Netherlands Institute for Radio Astronomy, Postbus 2, 7990 AA, Dwingeloo, The Netherlands
[4] Kapteyn Astronomical Institute, University of Groningen, P.O. Box 800, 9700 AV, Groningen, The Netherlands
[5] Max-Planck Institut für Astronomie, Königstuhl 17, D-69117, Heidelberg, Germany
Received 2015 January 12; accepted 2015 June 10; published 2015 July 15

ABSTRACT

Gas velocity dispersions provide important diagnostics of the forces counteracting gravity to prevent collapse of the gas. We use the 21 cm line of neutral atomic hydrogen (H I) to study H I velocity dispersion ($\sigma_{\rm H\,I}$) and H I phases as a function of galaxy morphology in 22 galaxies from The H I Nearby Galaxy Survey. We stack individual H I velocity profiles and decompose them into broad and narrow Gaussian components. We study the H I velocity dispersion and the H I surface density, $\Sigma_{\rm H\,I}$, as a function of radius. For spirals, the velocity dispersions of the narrow and broad components decline with radius and their radial profiles are well described by an exponential function. For dwarfs, however, the profiles are much flatter. The single Gaussian dispersion profiles are, in general, flatter than those of the narrow and broad components. In most cases, the dispersion profiles in the outer disks do not drop as fast as the star formation profiles derived in the literature. This indicates the importance of other energy sources in driving $\sigma_{\rm H\,I}$ in the outer disks. The radial surface density profiles of spirals and dwarfs are similar. The surface density profiles of the narrow component decline more steeply than those of the broad component, but not as steep as what was found previously for the molecular component. As a consequence, the surface density ratio between the narrow and broad components, an estimate of the mass ratio between cold H I and warm H I, tends to decrease with radius. On average, this ratio is lower in dwarfs than in spirals. This lack of a narrow, cold H I component in dwarfs may explain their low star formation activity.

Key words: galaxies: dwarf – galaxies: fundamental parameters – galaxies: ISM

1. INTRODUCTION

Studies of the shapes of the velocity profiles of neutral atomic hydrogen (H I) offer valuable information about the kinematical properties and phase structure of the interstellar medium (ISM) of galaxies (van der Kruit & Shostak 1982, 1984; Shostak & van der Kruit 1984; Young & Lo 1996, 1997a, 1997b; Braun 1997; de Blokx & Walterx 2006; Petric & Rupen 2007). However, the interpretation of the shapes of H I velocity profiles requires careful analysis to avoid confusion between the intrinsic shapes of the profiles, data artifacts and effects related to beam smearing or major bulk motions. The knowledge of the spatial distribution, variation and radial properties of the shapes of the profiles are important to understand the inter-relationship between gas properties and energetic processes such as star formation. In a previous paper (Ianjamasimanana et al. 2012), we reported on the shapes of stacked H I velocity profiles, averaged over the disks of galaxies from The H I Nearby Galaxy Survey (THINGS, Walter et al. 2008).

This paper investigates the shapes of the stacked profiles as a function of radius. Earlier work has also reported on this. For example, Kamphuis & Sancisi (1993) and Petric & Rupen (2007) found radially decreasing H I velocity dispersions in the face-on galaxies NGC 6946 and NGC 1058, respectively. Braun (1997) analyzed the H I emission spectra of 11 nearby spiral galaxies at a resolution of ∼150 pc and found filamentary structures, forming a so-called *High Brightness Network* (HBN). This HBN has a narrow line core with a velocity FWHM of less than ∼6 km s^{-1}, superposed on broad Lorentzian wings having a velocity FWHM extending up to ∼30 km s^{-1}. The HBN contains about 60%–90% of the total H I flux within the optical radius, r_{25}, but becomes less dominant or disappears in the outer disk. A simple radiative transfer modeling of the HBN indicates that its kinetic temperature increases with radius. Braun (1997) attributed the HBN to the Cold Neutral Medium (CNM) phase of the ISM.

In a recent study, Tamburro et al. (2009) analyzed the H I profiles of 11 face-on and intermediately inclined galaxies from THINGS, with the aim of understanding the physical mechanisms that determine the linewidth of the profiles. Tamburro et al. (2009) used second-moment values (i.e., intensity-weighted standard deviation of line of sight velocities) as tracers of the random motion of gas in the galaxies. These values decrease with radius from $\gtrsim$20 to ∼5 km s^{-1}. Tamburro et al. (2009) also reported that their sample exhibits a characteristic velocity dispersion value of 10 ± 2 km s^{-1} at r_{25}. By comparing the predicted energy input from different physical mechanisms with the gas kinetic energy inferred from the observed linewidth of the profiles, they concluded that star formation is the dominant mechanism that determines the width of the profiles inside r_{25}. Outside this radius, ultraviolet (UV) heating from extragalactic sources or magneto-rotational instability (MRI) were proposed to be likely candidates that set the widths of the profiles.

Stilp et al. (2013) also analyzed the shapes of H I velocity profiles in a sample of 23 galaxies from the THINGS and the VLA-ANGST (Ott et al. 2012) surveys. They applied a similar stacking method as we did in our previous analysis but they used a different interpretation of the shapes of the profiles. By fitting single Gaussians to the stacked profiles, they concluded

that the profiles can be described by a central narrow peak with a velocity width of ~6–10 km s^{-1} and wings to either side of the Gaussian core containing ~10%–15% of the total flux. The wings were attributed to turbulence driven by star formation feedback, mainly supernova explosions.

In our previous paper, we constructed high signal-to-noise ratio (S/N) profiles, called super profiles, by stacking individual profiles. We identified a sample of 22 galaxies from the THINGS sample where systematic effects from beam smearing, major bulk motions or individual asymmetric profiles play no large role. We refer the reader to Ianjamasimanana et al. (2012) for a detailed discussion of this. The main results are summarized below. The shapes of the super profiles are well described by the sum of a narrow and broad Gaussian components, with an average velocity dispersion of 7 $\pm$ 2 km s^{-1} and 17 $\pm$ 4 km s^{-1}, respectively. The super profile parameters (velocity dispersions and mass ratios between the broad and narrow components) correlate with metallicity and FUV–NUV colors.

Here we extend this work by analyzing the shapes of the super profiles as a function of radius in the 22 galaxies from Ianjamasimanana et al. (2012). In Section 2, we present the method and motivation for the analysis. In Section 3.1, we present measurements of the velocity dispersion as a function of radius. In Section 3.2, we compare our measured velocity dispersion values with those from the literature. In Section 3.3, we analyze the surface density of the single Gaussian, the narrow and broad components as a function of radius. We give conclusions and summarize our results in Section 4.

2. MOTIVATION AND METHODOLOGY

The shapes of H I velocity profiles are largely influenced by the local conditions within galaxies. Energy from stellar winds, supernova explosions, and magnetic fields (through MRI), is constantly injected into the ISM and its effect on the H I can be investigated by analyzing the shapes of the H I velocity profiles. As the amount of energy from the ISM can be different from one location to another within galaxies, the shapes of the profiles are expected to vary accordingly. Here we will analyze the key parameters that characterize the shapes of the H I velocity profiles as a function of radius. These are the velocity dispersion, the mass ratio between the narrow and broad components, as well as their surface densities.

Gas velocity dispersion is an important parameter as it quantifies the amount of random motion of gas induced by different energy sources (Tamburro et al. 2009). This random motion provides pressure support and prevents gravitational collapse of the gas. Thus, knowing the appropriate value of gas velocity dispersion is crucial for disk stability analysis. In an ideal case (i.e., purely thermal energy injection, small beam size), the velocity dispersion is a direct tracer of the gas kinetic temperature. In practice though, other sources of turbulence can increase the linewidth from its purely thermal value. Due to the lack of concrete knowledge about the appropriate value of the H I velocity dispersion, it has usually been assumed to be independent of radius. In this paper, we derive the H I velocity dispersion as a function of radial position for our sample galaxies. Note that our velocity dispersions include both the contribution of the thermal and the turbulent velocity dispersion of the H I gas. In addition to the velocity dispersion analysis, if the narrow and broad Gaussian components can be associated with the CNM and the WNM, then the super profile shapes can be used to study the relative amount of the WNM and the CNM as a function of radius.

We fit the super profiles with a double Gaussian function as described in detail by Ianjamasimanana et al. (2012). We also include results from fitting with a single Gaussian. This will facilitate a direct comparison with previous estimates of H I velocity dispersion in the literature, which did not take into account the presence of multiple components in H I. We refer the reader to Ianjamasimanana et al. (2012) for a detailed description of the error analysis. In summary, we define the uncertainties in the data points of each super profile as

$$\sigma = \sigma_{\rm ch.map} \times \sqrt{N_{\rm prof}/N_{\rm prof,beam}} \quad (1)$$

where $\sigma_{\rm ch.map}$ is the rms noise level in one channel map, $N_{\rm prof}$ is the number of stacked profiles at a certain velocity V, and $N_{\rm prof,beam}$ is the number of profiles per beam.

Here, we investigate the shapes of the super profiles as a function of radius. We derive and fit super profiles within annular ellipses of 0.2 r_{25} width. We use the optical radius, r_{25}, as indicative of the radius within which star formation is efficient. We also include scaling by the radial scale length of the stellar light, r_D, taken from Hunter & Elmegreen (2004) and Leroy et al. (2008). In the following, we separate our sample into spirals and dwarfs following the definition by Leroy et al. (2008). Therefore, galaxies with rotation velocities $V_{\rm rot} \leqslant 125$ km s^{-1}, stellar masses $M_* \lesssim 10^{10}\,M_\odot$, and absolute B magnitude $M_B \gtrsim -20$ mag are classified as dwarfs, whereas the more massive ones are classified as spirals. With this definition, our sample includes 12 dwarf and 10 spiral galaxies.

3. RESULTS

3.1. Velocity Dispersion as a Function of Radius

Figure 1 shows the single Gaussian, narrow, and broad components' velocity dispersions as a function of radius, normalized by the optical radius, r_{25}, and the radial scale length, r_D. In most cases, the velocity dispersions decrease exponentially with radius. The single Gaussian velocity dispersion profiles tend to be flatter than those of the narrow and broad components. This behavior can be understood as follows. In the inner disks, both narrow and broad individual line profiles make equally important contributions to the shapes of the derived super profiles, resulting in super profiles with a narrow peak and broad wings. Single Gaussian fits to these super profiles give velocity dispersion values between those of the narrow and broad components. As we go further out in the disk, the contribution of the narrow component to the overall shape of the super profiles becomes less important and the shapes of the super profiles become more Gaussian (see Section 3.3). In this case, single Gaussian fits to the super profiles result in velocity dispersion values close to those of the broad components. In conclusion, the change in the relative importance of the narrow and broad components seems to be the reason why here and in previous work (e.g., Leroy et al. 2008), the H I velocity dispersions derived from single Gaussian fitting of H I profiles hardly decline with radius.

We fit the radial velocity dispersion profiles with an exponential function of the form $\sigma_0 \exp(-r/l)$, where σ_0 is the fitted value of the central velocity dispersion, and l is the scale length. The results of the fits are shown as dashed lines in Figure 1. Spiral galaxies exhibit a clear radial decline in velocity dispersion, which can be well fitted by the exponential

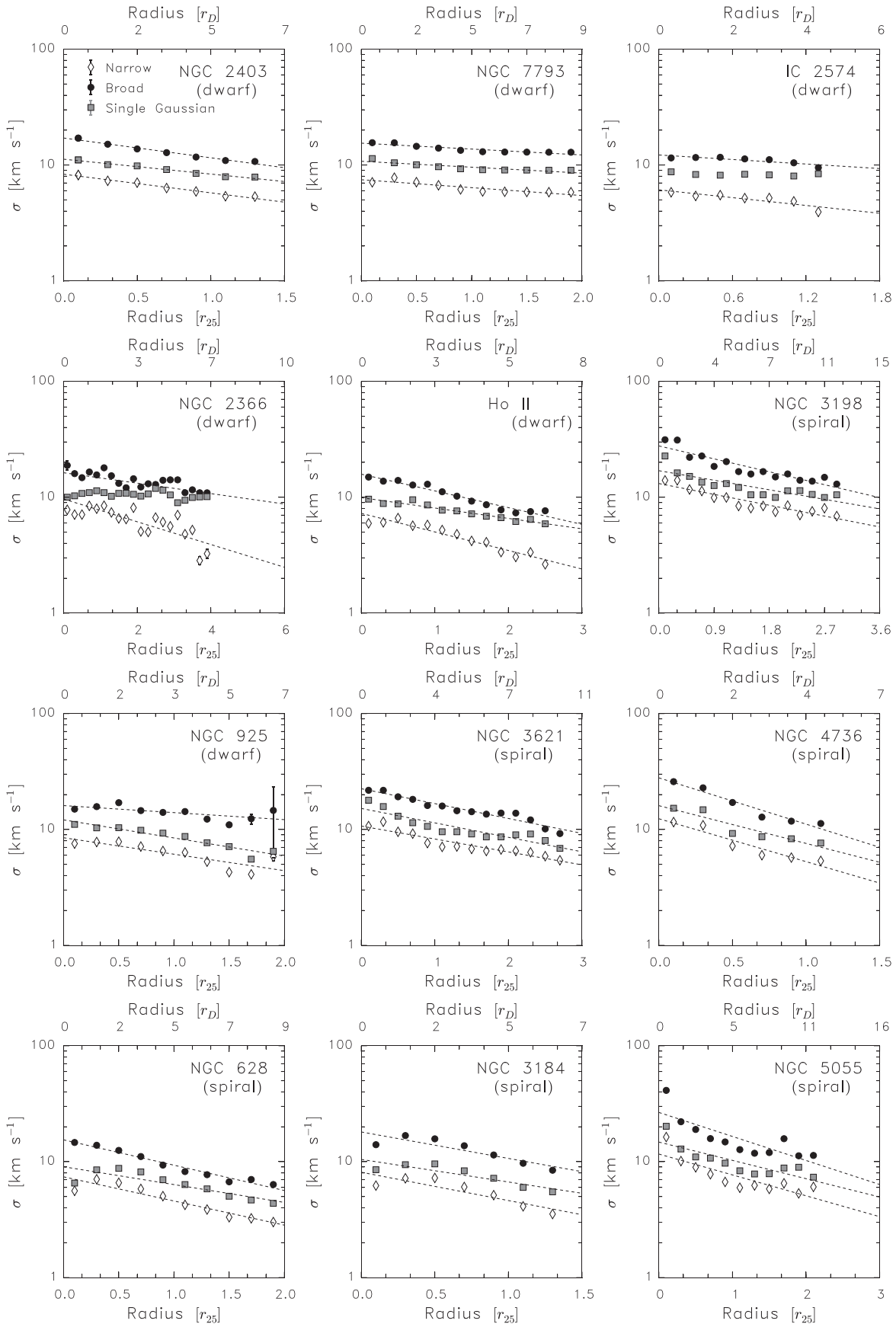

Figure 1. Velocity dispersions as a function of radius normalized by r_{25} and r_D. Black solid circle symbols represent the broad component velocity dispersions. The square gray symbols represent the velocity dispersions from the single Gaussian fits and the open diamond symbols show the velocity dispersions of the narrow component. The dashed lines are exponential fits. The uncertainties on the fitted velocity dispersion values are shown as error bars, though they are usually smaller than the size of the symbols.

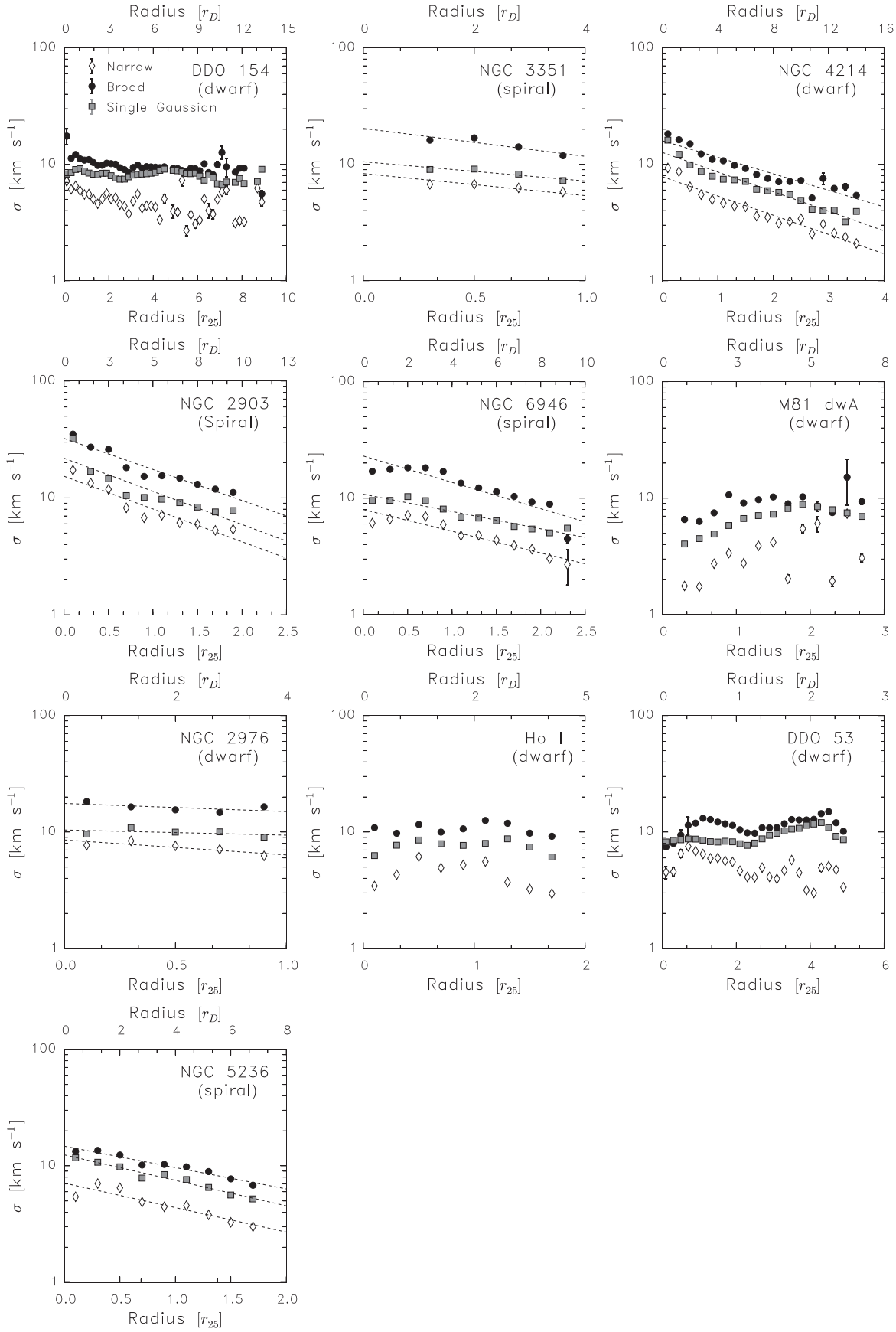

Figure 1. (Continued.)

Table 1
Fitted Velocity Dispersion Scale Lengths

Galaxy	r_{25} (kpc)	r_D (kpc)	l_{1g} (r_{25})	l_n (r_{25})	l_b (r_{25})
1	2	3	4	5	
NGC 2976	3.8	0.9	9.7 ± 10.6	3.4 ± 1.3	6.2 ± 4.4
NGC 2366	2.2	1.3	70.4 ± 84.1	4.4 ± 0.9	9.7 ± 2.0
HOII	3.3	1.2	4.8 ± 0.4	2.7 ± 0.2	3.0 ± 0.2
NGC 4214	2.9	0.7	2.6 ± 0.2	2.6 ± 0.2	3.1 ± 0.3
NGC 3184	12.0	2.4	2.2 ± 0.5	1.8 ± 0.4	1.9 ± 0.4
NGC 2403	7.4	1.6	3.4 ± 0.2	2.7 ± 0.2	2.5 ± 0.2
NGC 7793	5.9	1.3	8.5 ± 1.5	6.4 ± 1.1	8.5 ± 1.3
IC 2574	7.5	2.1	32.6 ± 25.0	3.9 ± 0.9	6.7 ± 1.7
NGC 628	10.4	2.3	2.8 ± 0.6	2.1 ± 0.3	2.0 ± 0.1
NGC 925	14.3	4.1	2.8 ± 0.3	3.1 ± 0.7	7.2 ± 3.0
NGC 2903	15.2	2.9	1.5 ± 0.3	1.5 ± 0.2	1.6 ± 0.2
NGC 3351	10.6	2.5	2.6 ± 0.8	3.8 ± 1.0	1.8 ± 0.6
NGC 5055	17.3	3.2	2.7 ± 0.6	2.4 ± 0.5	2.1 ± 0.5
NGC 4736	5.3	1.2	1.3 ± 0.3	1.2 ± 0.2	1.1 ± 0.1
NGC 3198	13.0	3.2	4.7 ± 0.9	4.2 ± 0.5	3.5 ± 0.4
NGC 3621	9.4	2.6	3.5 ± 0.4	3.9 ± 0.4	3.4 ± 0.2
NGC 6946	9.9	2.5	2.9 ± 0.3	2.3 ± 0.3	1.9 ± 0.3
NGC 5236	10.1	2.5	2.0 ± 0.1	2.1 ± 0.3	2.4 ± 0.2

Notes. Column 1: name of galaxy; Column 2: the optical radius, r_{25}, in units of kpc, adopting the distance in Walter et al. (2008); Column 3: the radial scale length, r_D, in units of kpc derived by Hunter & Elmegreen (2004) and Leroy et al. (2008); Column 4: velocity dispersion scale lengths from the single Gaussian fit; Column 5: velocity dispersion scale lengths of the narrow component; Column 6: velocity dispersion scale lengths of the broad component. Bold font indicates spiral galaxies, whereas normal font represents dwarf galaxies (adopting the definition of Leroy et al. 2008).

function. However, dwarf galaxies show flatter radial velocity dispersion profiles. Ho I, M81 dwA, DDO 53, and DDO 154 have flat profiles, giving unrealistically large scale lengths ($l \gg r_{25}$). For this reason, the fit for these galaxies are not shown in Figure 1. We list the scale length values for each galaxies in Table 1. Note that, for some galaxies, the results of the exponential fits depend on the radial range being fitted. For example, for NGC 3621, NGC 5055, NGC 2903, and NGC 3198 the radial decline starts to flatten at about the optical radius. Thus fitting only those points inside r_{25} will give a steeper slope. Here we fit the entire radial range.

We compare the velocity dispersion scale lengths of the broad and narrow components in Figure 2. We fit a linear function to this relation and we find a slope of ∼0.8, which indicates that the ratio between the velocity dispersion of the broad and narrow components is roughly constant with radius. The average velocity dispersion ratio between the narrow and broad component is $\langle \sigma_n/\sigma_b \rangle = 0.46 \pm 0.08$.

Figure 3 shows histograms of the velocity dispersion values measured in radial bins for spiral and dwarf galaxies in our sample. Note that here we exclude values within 0.2 r_{25} where beam smearing and streaming motions are expected to play a role as reported by Caldú-Primo et al. (2013). We fit the histograms with a Gaussian function; the results of the fit are shown in Table 2. As shown in the histograms and in Table 2, spirals and dwarfs have roughly the same mean velocity dispersion values, with $\langle \sigma_{1G} \rangle \simeq 8$ km s^{-1}. This is somewhat smaller than previous estimates of the single Gaussian velocity dispersion of the THINGS galaxies. Leroy et al. (2008) found $\langle \sigma_{1G} \rangle \simeq 11 \pm 3$ km s^{-1}, whereas Ianjamasimanana et al. (2012)

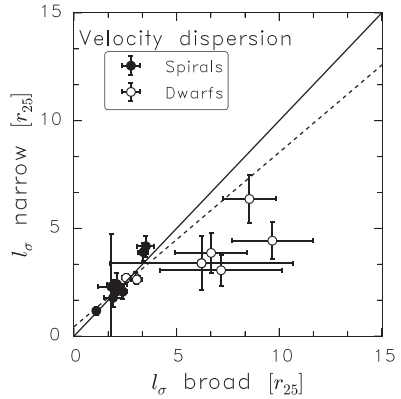

Figure 2. Comparison of the scale length of the broad and the narrow components. The dashed line is a linear fit to the data points. The solid line represents the line of equality. Note that Ho I, M81 dw A, DDO 154 and DDO 53 are not shown in this plot as their radial velocity dispersion profiles are not exponential.

and Caldú-Primo et al. (2013) found $\langle \sigma_{1G} \rangle \simeq 13 \pm 4$ km s^{-1} and 12 ± 3 km s^{-1}, respectively. The difference can be explained by our use of natural residual scaled cubes as opposed to non-residual scaled cubes adopted by Leroy et al. (2008) and Ianjamasimanana et al. (2012). E.g., for NGC 3184, the $\langle \sigma_{\rm H\,I} \rangle$ from residual-scaled cubes and non-residual scaled cubes differ by ∼3 km s^{-1}.The effects of residual scaling on H I velocity dispersion are analyzed in detail in a subsequent paper; but see also Stilp et al. (2013). Caldú-Primo et al. (2013) used residual-scaled cubes but considered a somewhat different radial range than is adopted in our analysis. They measured velocity dispersions of 12 spiral galaxies in regions where CO is present, mostly in the inner 60% of the optical radius. The radial range being considered here is larger than that of Caldú-Primo et al. (2013), explaining why our mean dispersion value is smaller than theirs since we include more points from the outer disks where velocity dispersions tend to be smaller. We find, for spirals, $\langle \sigma_{1G} \rangle \simeq 11 \pm 2$ km s^{-1} and $\langle \sigma_{1G} \rangle \simeq 8 \pm 2$ km s^{-1} inside and outside 0.6 r_{25}, respectively. This is consistent with the result of Caldú-Primo et al. (2013).

Although spirals and dwarfs have roughly the same $\langle \sigma_{1G} \rangle$ value, spirals have broader σ_{1G} distribution than dwarfs as shown in Figure 3. This may be caused by the effects of the presence of spiral arms or bars in spiral galaxies. Observational evidence for the effects of spiral arms on velocity dispersion has been presented by e.g., Shostak & van der Kruit (1984) for NGC 628. They found that the H I velocity dispersion of NGC 628 was ∼10 km s^{-1} in the spiral arms and ∼7 km s^{-1} in the interarm regions.

To have an overall representation of the radial velocity dispersion trend of the sample, we fit the complete set of radial velocity dispersion profiles with a single exponential function. Note that we exclude M81 dwA, DDO 154, Ho I, DDO 53 from this analysis due to their flat profiles. We further exclude IC 2574 and NGC 2366 as their single Gaussian velocity dispersion profiles are also flat. We try to remove the scatter between individual radial profiles by applying a normalization technique similar to the one presented in Schruba et al. (2012). That is, we normalize the velocity dispersions so that an exponential fit to the profiles has a value of unity at 0.6 r_{25}. Note that the choice of this value is arbitrary. This normalization technique removes galaxy-to-galaxy variation. We also fit the normalized radial velocity dispersion profiles with a

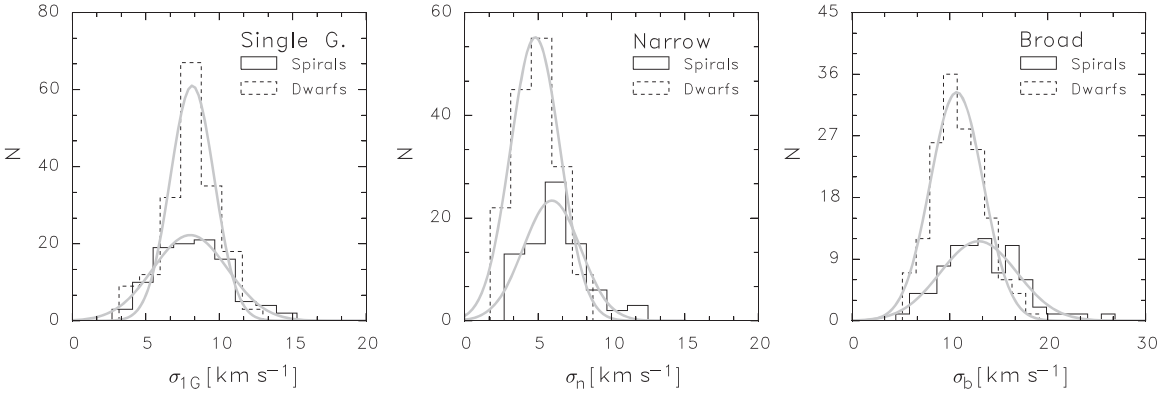

Figure 3. Histograms of individual points in the radial velocity dispersion profiles of dwarf and spiral galaxies. Points in the inner 0.2 r_{25} are excluded as they are mostly affected by beam smearing and streaming motions.

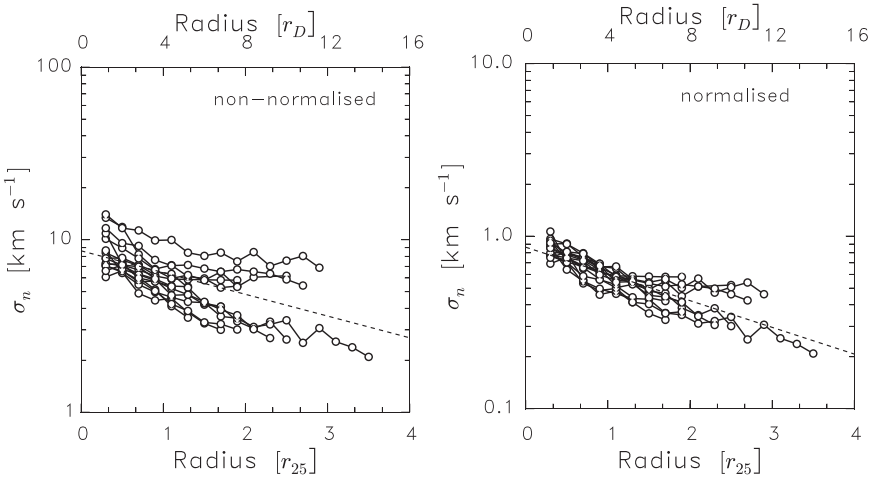

Figure 4. Combined (narrow component) radial velocity dispersion profiles before (left panel) and after (right panel) the normalization described in Section 3.1.

Table 2
Results of Gaussian Fits to the Histograms of Velocity Dispersion Values Measured in Radial Bins

	Single Gaussian $\langle\sigma_{1G}\rangle$ (km s^{-1})	Narrow $\langle\sigma_n\rangle$ (km s^{-1})	Broad $\langle\sigma_b\rangle$ (km s^{-1})
Spirals:	8.0 ± 2.5	5.9 ± 1.9	12.9 ± 3.9
Dwarfs:	8.2 ± 1.5	4.8 ± 1.7	10.7 ± 2.7

Table 3
Fitted Scale Lengths of Combined Radial Velocity Dispersion Profiles

Non-normalized			Normalized		
l_{1G} (r_{25})	l_n (r_{25})	l_b (r_{25})	l_{1G} (r_{25})	l_n (r_{25})	l_b (r_{25})
4.1 ± 2.1	3.5 ± 1.8	3.6 ± 3.8	3.7 ± 0.1	2.8 ± 0.1	3.0 ± 0.2

Note. The errors shown in the table are rms errors (i.e., scatter around best fit values).

single exponential function. We illustrate, for the narrow component, the combined radial profiles before and after normalization in Figure 4. We show the fitted scale lengths of the combined radial velocity dispersion profiles before and after normalization in Table 3. As expected, the (combined) normalized profiles show smaller scatter than the non-normalized ones. After the normalization, the scatter has decreased by more than 90%, whereas the fitted scale length values before and after the normalization agree within 20%. Thus, the scatter in the combined radial profiles is caused by galaxy-to-galaxy variation.

3.2. Comparison with Literature Values

Zhang et al. (2012) analyzed the variations of the H I power spectral index with channel width, for a sample of nearby dIrr galaxies, and suggested that the turbulent velocity dispersion of the coolest H I ($\lesssim$600 K) should not exceed $\sim$5 km s^{-1}. For dwarf galaxies in our sample, we also find an average value of $\sim$5 km s^{-1}. For spirals, this value is somewhat higher, but this can be explained by the higher energy input into the ISM in these galaxies.

A radial dependency of H I velocity dispersions has previously been reported in the literature. Dickey et al. (1990) and Petric & Rupen (2007) studied the H I kinematics of the face-on spiral galaxy NGC 1058 and found a radial decline of H I velocity dispersion from $\sim$12 km s^{-1} in the inner part to $\sim$6 km s^{-1} in the outer part. Boulanger & Viallefond (1992) and Boomsma et al. (2008) also found a radial fall-off of H I velocity dispersion for the face-on spiral galaxy NGC 6946. As already mentioned, Tamburro et al. (2009) analyzed

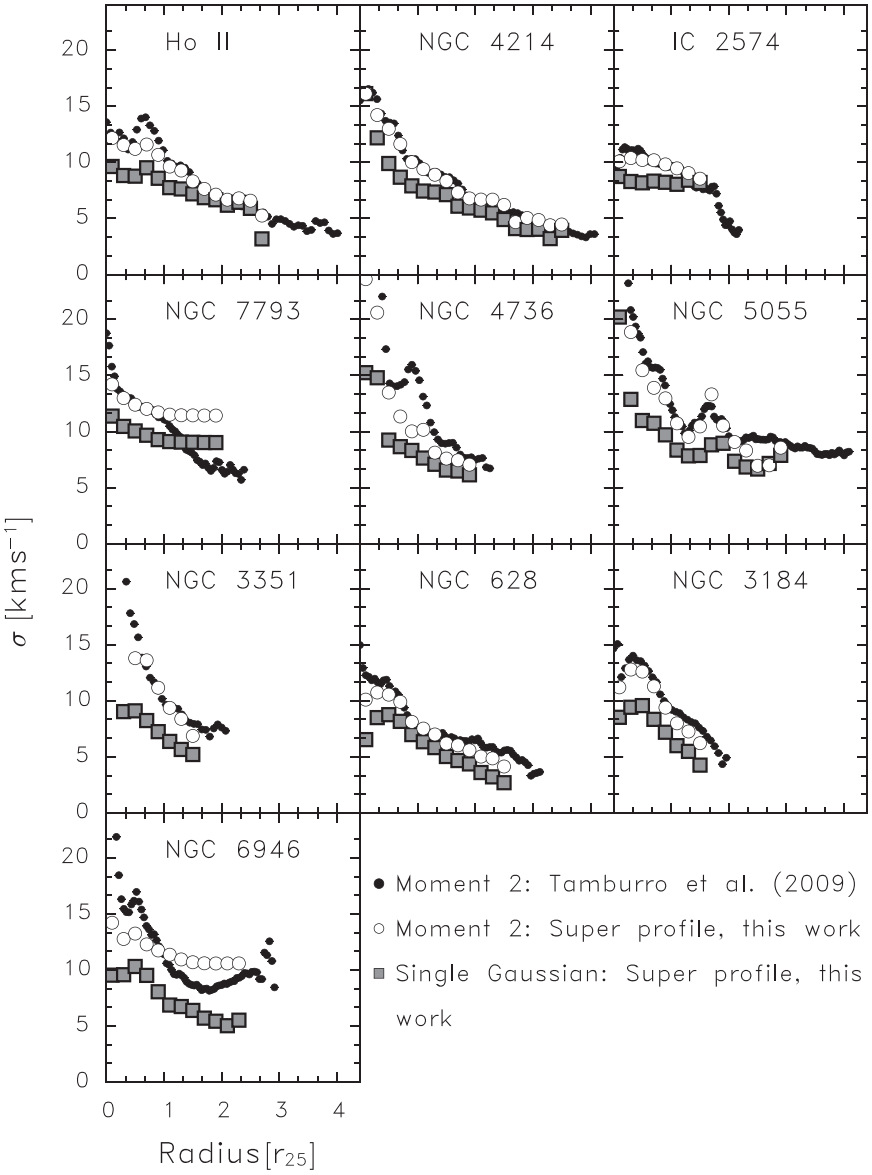

Figure 5. Comparison of our velocity dispersions with those derived in Tamburro et al. (2009). The solid black symbols represent the Tamburro et al. (2009) radial velocity dispersion profiles, derived from second moment maps. The square symbols are single Gaussian dispersions from our super profiles. The open circle symbols are second moment values calculated from the observed, total super profiles (i.e., no separation into broad and narrow components).

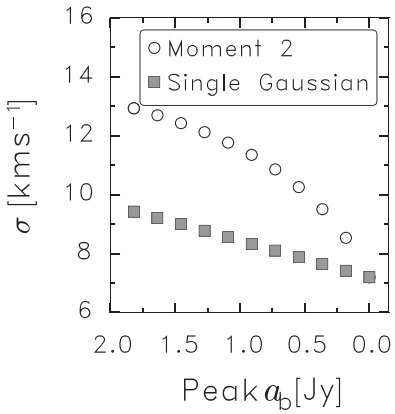

Figure 6. Testing the dependence of single Gaussian dispersion and second moment values on the strength of profile wings. Open circle symbols: second moment values. Square symbols: single Gaussian velocity dispersions. a_b: broad component amplitude.

the radial H I second moment profiles of 11 THINGS galaxies (all but one galaxy are also in our sample), and found that all exhibited a clear radial decline. Our single Gaussian velocity dispersion profiles can be directly compared to those presented in Boomsma et al. (2008) and Tamburro et al. (2009). For NGC 6946, the radial profile from Boomsma et al. (2008) shows a steep drop in velocity dispersion, followed by a linear decrease from about the optical radius to their outermost observed radius. Our velocity dispersion profile and that from Tamburro et al. (2009), however, show a continual decline from ~0.7 r_{25} to ~1.8 r_{25} and then start to level off.

We overplot our single Gaussian velocity dispersion profiles with the second moment velocity values of Tamburro et al. (2009) in Figure 5. Note that, in some cases, the radial velocity dispersion profiles of Tamburro et al. (2009) go further in radius than ours. This is because we have been more restrictive in fitting only high S/N profiles. We do not always find good agreement between our measured velocity dispersions and

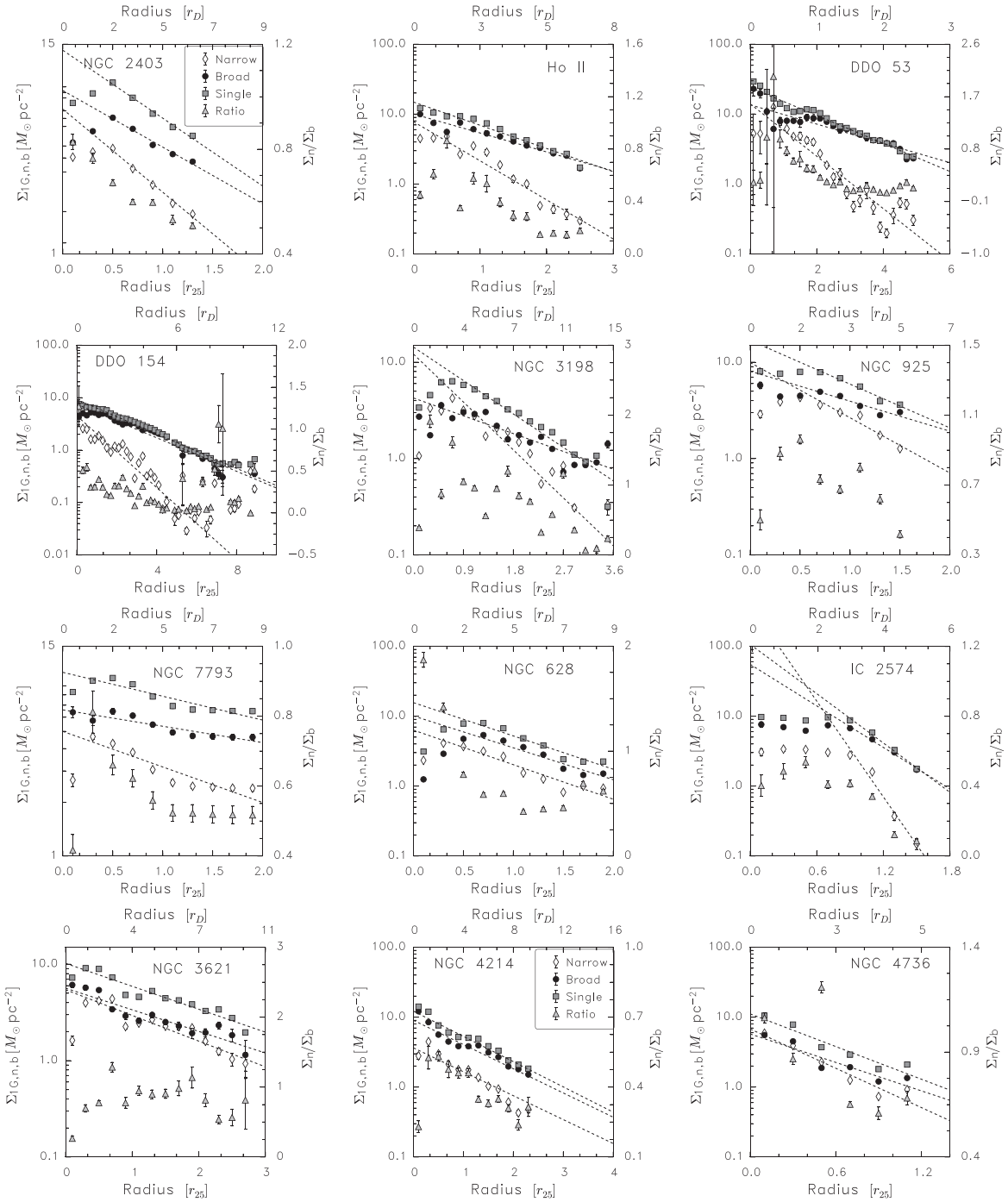

Figure 7. Open diamond symbols: surface density of the narrow component; solid black circle symbols: surface density of the broad component; square gray symbols: surface density of the single Gaussian component; triangle gray symbols: ratio between the surface densities of the narrow and broad components; dashed lines: exponential fits.

those from Tamburro et al. (2009), especially in the central parts of galaxies where our velocity dispersions tend to be smaller. This can be explained by the fact that the shapes of the velocity profiles in the inner disks of galaxies are usually strongly non-Gaussian. For a perfectly Gaussian profile, the second moment value and the single Gaussian dispersion would be equal. However, for a velocity profile with prominent wings, the second moment value would be higher than that of the single Gaussian dispersion.

In Figure 5, we also show second moment values derived from the observed, total super profiles (i.e., no separation into broad and narrow components was made). The offset between the single Gaussian dispersions and the second moment values become smaller with increasing radius and, for most galaxies, the two dispersions start to agree at a certain radius. This behavior is due to the shapes of the profiles becoming more and more Gaussian toward larger radius. The radius where the values start to agree may indicate the point beyond which only the WNM is dominant.

To better understand the behavior of the second moment values as a function of profile shape, we proceed as follows. We take the fitted super profile of NGC 3184 at 0.3 r_{25} (this is a

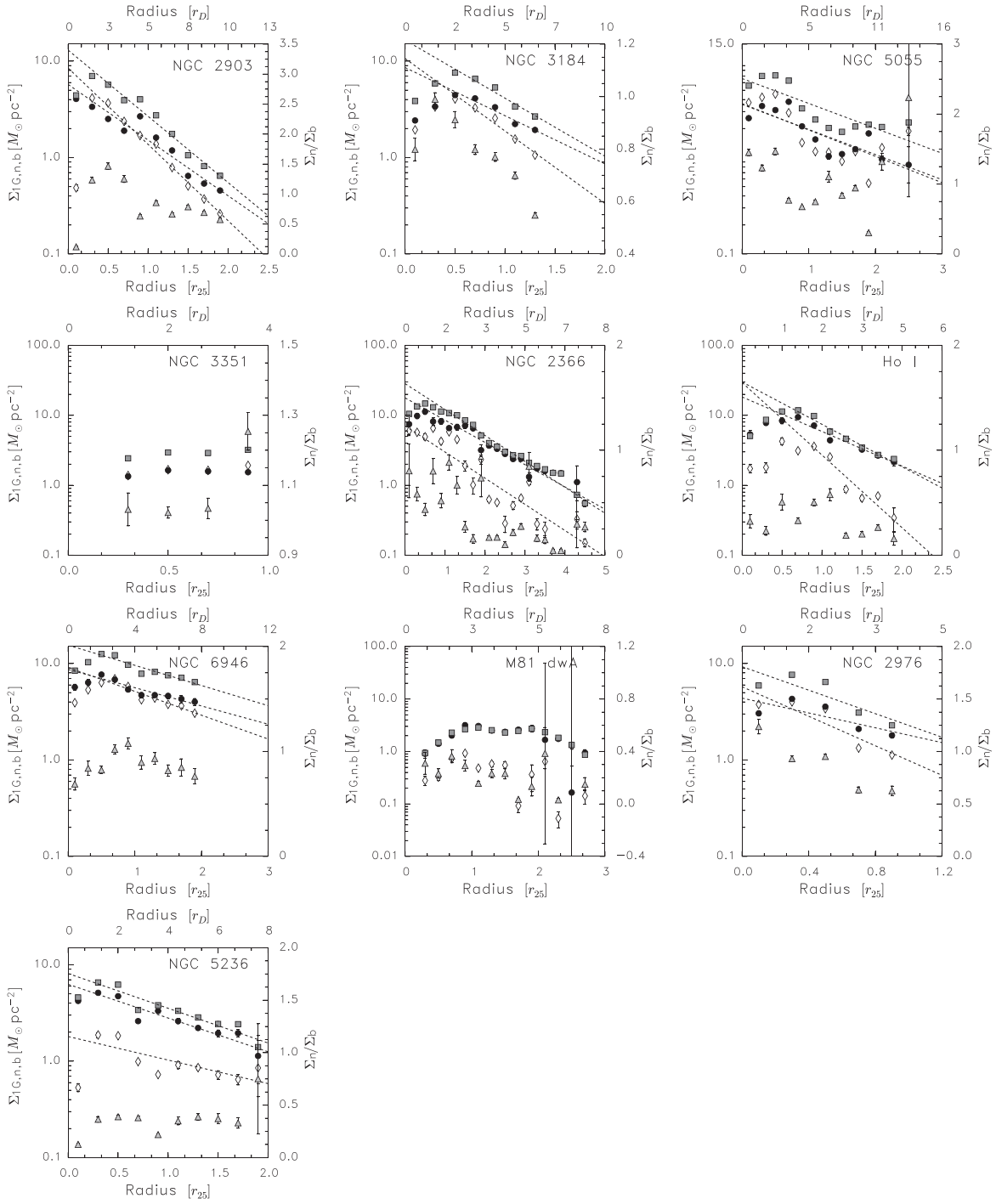

Figure 7. (Continued.)

typical non-Gaussian super profile with broad and narrow components of a face-on galaxy). We derive a single Gaussian dispersion and a second moment value from it. We then gradually suppress the wings of the profile by decreasing the broad component amplitude while keeping the narrow component parameters fixed. We re-measure the single Gaussian and the second moment values. We do this until the broad component is completely suppressed and we are left with a single Gaussian profile. We plot the derived second moment velocity values and single Gaussian velocity dispersions as a function of the broad component amplitude in Figure 6. As expected, the disagreement between the two values becomes smaller with decreasing wing's strength. They are identical when the profiles are perfect Gaussians. It is also worth noting that the single Gaussian dispersion is less affected by the profile wings than the second moment value.

3.3. Surface Density as a Function of Radius

In addition to measuring velocity dispersions, we can also use the super profiles to investigate the surface densities of the various components. Here, we present radial surface density

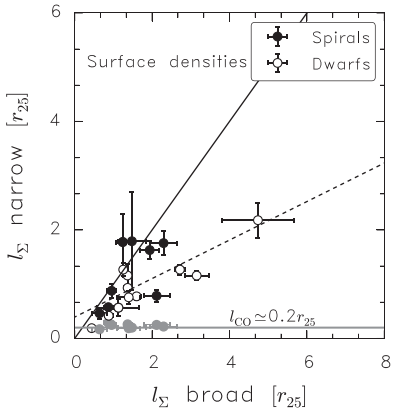

Figure 8. Comparison of the scale lengths derived from the narrow and broad component surface density profiles. The solid line is a line of equality and the dashed line is a linear fit with a slope of 0.6. Gray points are CO surface density scale length by Schruba et al. (2012); the mean CO scale length is shown as a horizontal solid line.

Table 4
Fitted Surface Density Scale Lengths

Galaxy	r_{25} (kpc)	r_D (kpc)	l_{1g} (r_{25})	l_n (r_{25})	l_b (r_{25})
1	2	3	4	5	
NGC 2976	3.8	0.9	0.5 ± 0.1	0.4 ± 0.1	0.6 ± 0.1
NGC 2366	2.2	1.3	1.2 ± 0.0	1.2 ± 0.2	1.4 ± 0.1
HOII	3.3	1.2	1.1 ± 0.1	0.6 ± 0.0	1.4 ± 0.1
NGC 4214	2.9	0.7	1.2 ± 0.1	0.9 ± 0.1	1.3 ± 0.1
NGC 3184	12.0	2.4	0.7 ± 0.1	0.6 ± 0.1	0.9 ± 0.1
NGC 2403	7.4	1.6	1.1 ± 0.1	0.9 ± 0.1	1.4 ± 0.1
NGC 7793	5.9	1.3	3.2 ± 0.5	2.2 ± 0.3	4.7 ± 0.9
IC 2574	7.5	2.1	0.4 ± 0.0	0.2 ± 0.0	0.4 ± 0.0
DDO154	1.2	0.8	2.6 ± 0.1	1.3 ± 0.1	2.7 ± 0.1
NGC 628	10.4	2.3	0.9 ± 0.1	0.9 ± 0.1	1.0 ± 0.1
HOI	1.8	0.8	0.7 ± 0.0	0.5 ± 0.1	0.8 ± 0.1
NGC 925	14.3	4.1	1.0 ± 0.1	0.8 ± 0.1	1.4 ± 0.3
NGC 2903	15.2	2.9	0.6 ± 0.0	0.6 ± 0.0	0.8 ± 0.1
NGC 5055	17.3	3.2	1.8 ± 0.6	2.0 ± 1.1	1.5 ± 0.4
DDO53	0.4	0.7	2.2 ± 0.1	1.2 ± 0.1	3.2 ± 0.3
NGC 4736	5.3	1.2	0.6 ± 0.1	0.5 ± 0.1	0.6 ± 0.1
NGC 3198	13.0	3.2	1.3 ± 0.0	1.0 ± 0.1	1.6 ± 0.2
NGC 3621	9.4	2.6	1.8 ± 0.2	1.6 ± 0.2	2.0 ± 0.3
NGC 6946	9.9	2.5	2.4 ± 0.4	1.6 ± 0.2	3.5 ± 0.9
NGC 5236	10.1	2.5	1.2 ± 0.2	2.2 ± 1.0	1.3 ± 0.2

Notes. Column 1: name of galaxy; Column 2: the optical radius, r_{25}, in units of kpc, adopting the distance in Walter et al. (2008); Column 3: the radial scale length, r_D, in units of kpc derived by Hunter & Elmegreen (2004) and Leroy et al. (2008); Column 4: surface density scale lengths from the single Gaussian fit; Column 5: surface density scale lengths of the narrow component; Column 6: surface density scale lengths of the broad component. Bold font indicates spiral galaxies, whereas normal font represents dwarf galaxies (adopting the definition of Leroy et al. 2008).

profiles of the single Gaussian component, $\Sigma_{1G}(R)$, the narrow component, $\Sigma_n(R)$, the broad component, $\Sigma_b(R)$, and the $\Sigma_n(R)/\Sigma_b(R)$ ratio. If the narrow and broad components represent the CNM and the WNM, then, the Σ_n/Σ_bratio represents the surface density ratio between the CNM and the WNM. Theoretical models (Wolfire et al. 2003) predict the CNM/WNM ratio to decrease as a function of radius due to a radially declining thermal pressure of the H I gas. This has also been confirmed by observations of 11 nearby spiral galaxies by Braun (1997).

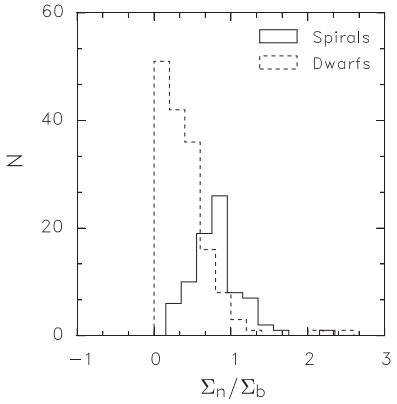

Figure 9. Histograms of Σ_n/Σ_b measured in radial bins.

Figure 7 shows Σ_{1G}, Σ_n, Σ_b, and Σ_n/Σ_b as a function of radius. We fit a single exponential function to the surface density profiles to facilitate comparisons with CO surface density profiles from Schruba et al. (2012). These authors fit a single exponential function to the CO surface density profiles of galaxies from the HERA CO-Line Extragalactic Survey (Leroy et al. 2009), a CO $J = 2 \rightarrow 1$ survey which covers most of the THINGS sample. Exponential H I surface density profiles were already found for late-type dwarf galaxies (Swaters et al. 2002). Here, we find that the radial decline in surface densities can be reasonably described by the exponential function. The narrow component surface densities tend to have smaller scale lengths than those of the broad component. The single Gaussian surface densities decline radially with a scale length somewhere between those of the narrow and broad components. We show a comparison of the scale lengths of the narrow and broad component's surface density profiles in Figure 8 and Table 4.

To test whether the surface density of the narrow component traces the surface density of molecular gas, we compare the narrow component's surface density scale length with that of a tracer of the molecular gas component. Schruba et al. (2012) found that the integrated CO intensities in their sample (a sample of 33 nearby spiral galaxies) decrease exponentially with a scale length of $\sim 0.2\ r_{25}$. This is much steeper than the scale length of the narrow component's surface density that we find in this analysis ($l \sim 1.1\ r_{25}$). This result suggests that the formation of cold H I is not a sufficient condition for the formation of molecular gas (Schaye 2004). As put forward by Young & van Zee (2003), it is also possible that there is a delay between the formation of cold H I and H_2. This is because factors such as pressure, column density, metallicity, play a role in the transition from H I to H_2 (Elmegreen 1993; Honma et al. 1995). Another possibility is that, in some regions, even if H_2 formation proceeds after the formation of cold H I, the H_2 molecule is subsequently destroyed by FUV radiation (Elmegreen 1993).

The Σ_n/Σ_b ratio tends to decrease with radius. In a similar analysis, Braun (1997) found that the fractional line flux of the HBN mentioned previously (attributed to the CNM) decreases abruptly near the optical radius, r_{25}. However, only about 20% of our sample galaxies show an abrupt decrease in the Σ_n/Σ_b near the optical radius. For most galaxies, the Σ_n/Σ_b ratio continually declines without a clear break. We attempted to fit

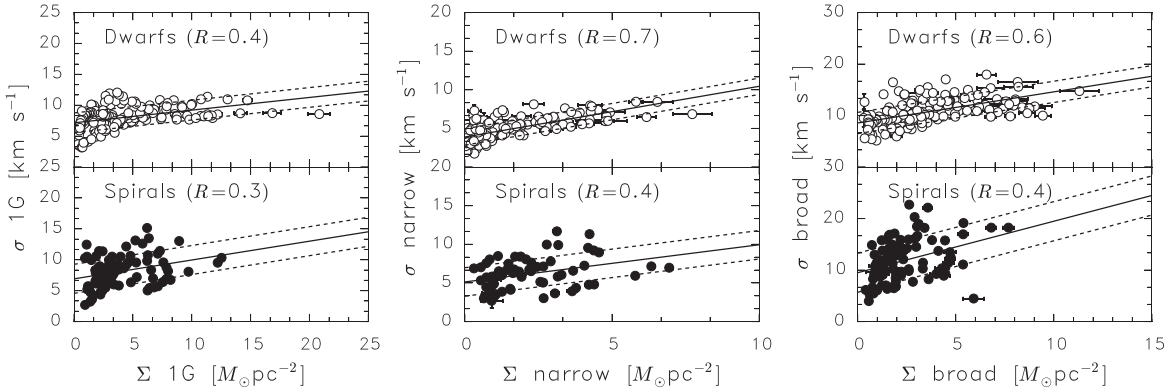

Figure 10. Comparison of the velocity dispersions and the surface densities of the single Gaussian (left panel), narrow (middle panel) and broad (right panel) components. The solid lines are linear fits to the data; the dashed lines are one-sigma rms scatters. *R* denotes the Pearson's rank correlation coefficients.

the super profiles with the sum of a Gaussian and a Lorentzian function, similar to Braun (1997) but we still did not find a clear break in the Σ_n/Σ_b profiles. This difference could be due to the fact that we fitted the super profiles with the sum of a Gaussian plus Lorentzian function with all parameters free rather than with the physical model assumed by Braun (1997). Investigation of this will be left as future work.

We compare the Σ_n/Σ_b ratio of dwarfs and spirals in Figure 9. On average, spirals have higher Σ_n/Σ_b ratio (0.8 ± 0.3) than dwarfs (0.4 ± 0.3), consistent with the results presented in Ianjamasimanana et al. (2012). We attribute the difference in Σ_n/Σ_b as an indication that the fraction of cold H I component is higher in spirals than in dwarfs.

Figure 10 shows a comparison of H I velocity dispersions and H I surface densities. Dwarf galaxies show stronger correlation, and less scatter, in the $\sigma_{\rm H\,I}\Sigma_{\rm H\,I}$ relation than spirals. Possibly this is due to the presence of extra morphological and kinematical features such as bars and spiral arms which are not present in dwarf galaxies. Confirmation of this needs the stacking of super profiles in the arms and inter-arm regions, which is beyond the scope of the current analysis. We use the Pearson's rank correlation coefficient, *R*, to quantify the strength of the correlation between $\sigma_{\rm H\,I}$ and $\Sigma_{\rm H\,I}$. In general, $\sigma_{\rm H\,I}$ and $\Sigma_{\rm H\,I}$ correlate better to each other for the narrow component than for the broad and the single Gaussian components. If the narrow component is associated with star formation as shown before by Young & Lo (1996) and de Blokx & Walterx (2006), then the correlation between $\sigma_{\rm H\,I}$ and $\Sigma_{\rm H\,I}$ may be driven by star formation. Correlation between $\sigma_{\rm H\,I}$ and $\Sigma_{\rm H\,I}$ has previously been reported in the literature (Shostak & van der Kruit 1984; Stilp et al. 2013). Shostak & van der Kruit (1984) found a positive correlation between $\sigma_{\rm H\,I}$ and $\Sigma_{\rm H\,I}$ for NGC 628. Since regions of higher $\Sigma_{\rm H\,I}$ usually correspond to regions of active star formation, Shostak & van der Kruit (1984) attributed the increase in $\sigma_{\rm H\,I}$, in regions of high $\Sigma_{\rm H\,I}$, as a result of energy input by stellar winds from OB stars, supernovae and expanding H II regions.

4. SUMMARY AND CONCLUSION

This paper presents a comparison of the radial variation of H I velocity dispersions and surface densities of the components of H I in spiral and dwarf galaxies. Spirals exhibit a clear radial decline in velocity dispersion, which can be well described by an exponential function. Dwarfs show flatter or flat radial velocity dispersion profiles. On average, though, we find that spiral and dwarf galaxies have similar H I velocity dispersion.

The radial velocity dispersion profiles derived from single Gaussian fits to stacked H I profiles (super profiles) tend to be flatter than those of the narrow and broad components, identified from a double Gaussian fit to the super profiles. In addition, the single Gaussian dispersion values approach those of the broad component at large radius, suggesting the broad component is dominant in the outer disks.

In general, the velocity dispersion profiles in the outer parts do not drop at the same rate as the star formation rate profiles analyzed by Tamburro et al. (2009). We therefore confirm their conclusion that star formation is not the main drivers of the H I dispersions in the outer disk of galaxies. Our measured H I dispersions are, however, somewhat smaller than the second moment values of Tamburro et al. (2009). This is because second moment values are sensitive to the shapes of the profiles and therefore do not always reflect the velocity dispersions.

In terms of surface densities, spiral and dwarf galaxies have similar radial behavior. We find that, except in the innermost part, the surface densities exponentially decrease with radius. This decrease is steeper for the narrow component than for the single Gaussian and broad components. The surface density ratio between the narrow and broad components also tend to decrease with radius. Identifying the narrow component with the CNM and the broad component with the WNM, this indicates that the fraction of gas in the cold phase tends to be higher in the inner parts of the galaxy disks. On average, dwarfs have a lower surface density ratio $(\Sigma_n/\Sigma_b = 0.4 \pm 0.3)$ than spirals $(\Sigma_n/\Sigma_b = 0.8 \pm 0.3)$, indicating that dwarf galaxies have a relatively lower amount of cold H I component than spiral galaxies. Finally, we find that $\sigma_{\rm H\,I}$ is correlated with $\Sigma_{\rm H\,I}$, which we interpret as a correlation with star formation given the relationship between $\Sigma_{\rm H\,I}$ and $\Sigma_{\rm SFR}$.

We thank the anonymous referee for constructive comments that have improved this paper. R.I. acknowledges funding from the South African National Research Foundation (NRF grant number MWA1203150687), a Postdoctoral Grant of the University of South Africa, and the PPI grant of the University of Cape Town. R.I.'s working visit to the Netherlands was supported by NRF-NWO exchange programme in "Astronomy, and Enabling Technologies for Astronomy." The work of W.J.G.d.B. was supported by the European Commission (grant FP7-PEOPLE-2012-CIG #333939).

REFERENCES

Boomsma, R., Oosterloo, T. A., Fraternali, F., et al. 2008, A&A, 490, 555
Boulanger, F., & Viallefond, F. 1992, A&A, 266, 37
Braun, R. 1997, ApJ, 484, 637
Caldú-Primo, A., Schruba, A., Walter, F., et al. 2013, AJ, 146, 150
de Blok, W. J. G., & Walter, F. 2006, AJ, 131, 363
Dickey, J. M., Hanson, M. M., & Helou, G. 1990, ApJ, 352, 522
Elmegreen, B. G. 1993, ApJ, 411, 170
Honma, M., Sofue, Y., & Arimoto, N. 1995, A&A, 304, 1
Hunter, D. A., & Elmegreen, B. G. 2004, AJ, 128, 2170
Ianjamasimanana, R., de Blok, W. J. G., Walter, F., & Heald, G. H. 2012, AJ, 144, 96
Kamphuis, J., & Sancisi, R. 1993, A&A, 273, L31
Leroy, A. K., Walter, F., Brinks, E., et al. 2008, AJ, 136, 2782
Leroy, A. K., Walter, F., Bigiel, F., et al. 2009, AJ, 137, 4670
Ott, J., Stilp, A. M., Warren, S. R., et al. 2012, AJ, 144, 123
Petric, A. O., & Rupen, M. P. 2007, AJ, 134, 1952
Schaye, J. 2004, ApJ, 609, 667
Schruba, A., Leroy, A. K., Walter, F., et al. 2012, AJ, 142, 37
Shostak, G. S., & van der Kruit, P. C. 1984, A&A, 132, 20
Stilp, A. M., Dalcanton, J. J., Warren, S. R., et al. 2013, ApJ, 765, 136
Swaters, R. A., van Albada, T. S., van der Hulst, J. M., & Sancisi, R. 2002, A&A, 390, 829
Tamburro, D., Rix, H.-W., Leroy, A. K., et al. 2009, AJ, 137, 4424
van der Kruit, P. C., & Shostak, G. S. 1982, A&A, 105, 351
van der Kruit, P. C., & Shostak, G. S. 1984, A&A, 134, 258
Walter, F., Brinks, E., de Blok, W. J. G., et al. 2008, AJ, 136, 2563
Wolfire, M. G., McKee, C. F., Hollenbach, D., & Tielens, A. G. G. M. 2003, ApJ, 587, 278
Young, L. M., & Lo, K. Y. 1996, ApJ, 462, 203
Young, L. M., & Lo, K. Y. 1997a, ApJ, 476, 127
Young, L. M., & Lo, K. Y. 1997b, ApJ, 490, 710
Young, L. M., van Zee, Lo, K. Y., et al. 2003, ApJ, 592, 111
Zhang, H.-X., Hunter, D. A., & Elmegreen, B. G. 2012, ApJ, 754, 29